CHAPTER 8

RDC for Membrane Proteins

JAMES J. CHOU

Department of Biological Chemistry and Molecular Pharmacology,
Harvard Medical School, Boston, MA 02115, USA
Email: james_chou@hms.harvard.edu

8.1 Introduction

Despite the tremendous success of cryo-electron microscopy (cryo-EM) and crystallography, especially lipidic cubic phase (LCP) crystallization, in visualizing membrane protein structures at high resolution, there are still areas of membrane proteins that have been rather inaccessible by these technologies. For example, the transmembrane domains (TMDs) of type I/II membrane proteins have historically occupied a "blind spot" in structural biology because they have been extremely difficult targets for crystallography.[1] The rapid advance in cryo-EM in the past decade has renewed much enthusiasm and effort to resolve single-pass membrane proteins that include TMDs. But these goals are still exceptionally challenging, as only a few successful examples have been reported thus far, *e.g.*, the cryo-EM structure of the TCR/CD3 complex containing ectodomains and TMDs, stabilized by chemical crosslinking.[2] The technical bottleneck remains. The TMD alone is too small for cryo-EM, but when being examined as a part of the full-length receptor, motion between the large ectodomain and the small TMD can pose a fundamental problem for cryo-EM particle averaging. Mounting evidence from structural and functional studies has shown that the TMDs of many single-pass membrane proteins are not passive membrane anchors but play essential roles in protein assembly and activation.[3–11] Other areas of membrane proteins that have resisted crystallization efforts are small viral membrane proteins such as viroporins.[12] Many membrane-proximal proteins or domains that are

New Developments in NMR No. 31
Residual Dipolar Couplings: Principles and Applications
Edited by Lishan Yao and Beat Vögeli

Published by the Royal Society of Chemistry, www.rsc.org

not embedded in the membrane are also difficult to visualize by crystallography or EM as they have the stringent requirement of being in a planar lipid bilayer environment to be conformationally and functionally relevant. For example, the membrane-proximal or juxtamembrane regions of signaling receptors often play essential roles in the function of these proteins,[6,13] but their structures are unknown for most of these type I/II membrane proteins. Moreover, how these receptors rest on the membrane before activation by the ligand is also largely unknown. These are areas where NMR can immediately contribute and fill the knowledge gaps.

In principle, NMR protocols that have been established for water-soluble proteins should be directly applicable to membrane proteins. These protocols, however, need to be tailored to account for the fundamental physical–chemical differences between membrane proteins and water-soluble proteins and the imperative for use of a model membrane medium. There are several issues that complicate solution NMR studies of membrane proteins. (1) Membrane proteins need to be solubilized in detergent micelles or detergent/lipid bicelles. We do not understand exactly how various types of detergents assemble a micelle around membrane proteins and thus cannot predict the effective size of a protein–micelle complex. Furthermore, the presence of very high concentrations of surfactants requires methods to suppress their NMR signals. (2) Amino acid sequences of membrane proteins have been optimized in nature in the membrane environment, and thus it is unclear whether detergent micelles fully mimic the lateral lipid pressure that a protein experiences in a true membrane. For α-helical membrane proteins, insufficient lipid pressure in detergent micelles could result in weaker helix–helix packing or increased internal "breathing" in solution. The internal dynamics would pose a problem for measuring long-range NOEs. (3) In general, membrane proteins contain many more methyl-bearing amino acids than water-soluble proteins, and most of the hydrophobic residues are lipid facing, unconfined to a unique chemical environment. These properties of membrane proteins result in a much smaller chemical shift dispersion of the methyl groups than that of water-soluble proteins (in which hydrophobic residues are strongly packed in the protein core). The crowded methyl spectrum poses a serious problem in assigning inter-helical NOEs, which requires unambiguous assignments of the methyl resonances.

One way to compensate for the lack of tertiary NOEs is measuring paramagnetic relaxation enhancement (PRE) restraints[14] and this approach has been used in the structural studies of several integral membrane proteins such as DsbB,[15] DAGK,[16] and OmpA.[17] PRE measurement involves measuring (using either 2D or 3D experiments) ^{1}H $R_2 + R_2^{\text{para}}$ for ^{1}H resonances that are broadened by a particular spin label and ^{1}H R_2 after reducing the unpaired electron with ascorbic acid. R_2^{para} is then used to derive distance restraints based on the known calibrations.[14] In addition to providing long-range distance restraints (12–25 Å), a major advantage of PRE is that the measurement and analysis are both simple and unambiguous if the

resonance assignments are accurate. The shortcoming of PRE is also obvious. The nitroxide spin label is ~8 Å long and is flexible like the lysine sidechain. Hence, PRE restraints have very large uncertainty, typically ±5 Å. It is therefore not useful for determining local or secondary structures. Nonetheless, a large number of unambiguous PRE restraints can compensate somewhat for their low precision. With existing knowledge of the local structures from NOE and RDCs, PRE restraints are useful in providing a low resolution global fold that can facilitate further NOE assignments.

The aforementioned technical problems have limited the amount of NMR restraints obtainable for membrane proteins. Hence, there has been major interest in developing protocols to include RDCs to improve the accuracy of membrane protein structure determination by NMR. One of the first applications was comparing the structures of a peptide fragment of the HIV-1 membrane fusion protein gp41 (residues 282–304) when bound to detergent micelles formed by DH_6PC (1,2-dihexanoyl-*sn-glycero*-3-phosphocholine) and to lipid–detergent bicelles comprising DMPC (1,2-dimyristoyl-*sn-glycero*-3-phosphocholine) and DH_6PC. The gp41 fragment forms an amphipathic helix residing in the headgroup region of phospholipids. By measuring backbone RDCs using a stretched polyacrylamide gel and including the RDCs in structure calculations, it was found that while the helix is straight when bound to the bicelles, the micelles induced a noticeable curvature in the bound helix.[18] This study demonstrated the advantage of bicelles over micelles for studying membrane proteins; it also suggested that although unambiguous identification of the weak curvature observed in the detergent micelle is generally not possible using NOEs and *J* couplings, it could be determined quantitatively by RDCs. After that, RDCs have been included in several structural studies of larger membrane proteins or domains such as the pentameric phospholamban,[19] the influenza M2 channel,[20] the DsbB,[15] and the diacylglycerol kinase (DAGK),[16] all of which used strained polyacrylamide gels for introducing weak alignment of membrane proteins. Since membrane proteins often contain helices that span the membrane and amphipathic domains that reside at the membrane–solvent interface, the structured regions can adopt a very different orientation relative to the lipid bilayer and defining the global orientation of these regions is precisely the forte of RDC analysis. Technical challenges, however, remain for RDC application to membrane proteins, including greater technical hurdle of protein alignment, the lower sensitivity of RDC measurement, and the complexity of protein dynamics in RDC analysis. This chapter provides a background review of these technical issues and existing solutions for addressing them.

8.2 Alignment Media for Membrane Proteins

As described in Section 3.3 of Chapter 3, the most effective method for weak alignment involves mixing the protein of interest with large particles that form stable liquid crystals at low concentrations (~1.5–5% w/v).[21] Bax and

Tjandra first demonstrated this method using DMPC–DH_6PC bicelle liquid crystals.[22] Subsequently, a number of different liquid crystals have been found to be suitable for aligning water-soluble proteins and the commonly used ones include filamentous phage particles,[23,24] poly(ethylene glycol)-based systems,[25] and cellulose crystallites.[26] These liquid crystals, however, could not be applied to membrane proteins reconstituted in detergent micelles or detergent–lipid bicelles due to incompatibility with the detergents. Apart from weak alignment in solution by steric collision, paramagnetic tags have been demonstrated to induce weak alignment for membrane proteins solubilized in detergent micelles or lipid–detergent bicelles (Figure 8.1A). For example, when fused to the EF-hand that coordinates the paramagnetic lanthanide ions (Yb^{3+} or Dy^{3+}), the HIV-1 Vpu reconstituted in DH_6PC micelles showed weak alignment that yielded ^{15}N–^{1}H dipolar couplings as large as 7.8 Hz.[27] The approach of the paramagnetic tag, however, has two short comings: (1) low magnitude of alignment and (2) requirement for protein modification that might cause problems for expression, purification, or reconstitution. Hence, there was substantial interest in developing robust alignment media suitable for RDC measurement of membrane proteins.

8.2.1 Strained Polyacrylamide Gel

One method to sterically induce protein alignment but without involving a liquid crystal is the strain-induced alignment in polyacrylamide gel (SAG).[28,29]

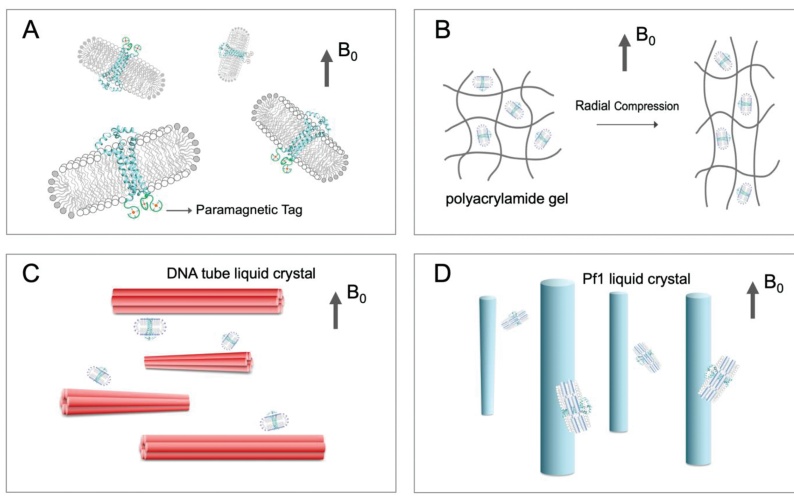

Figure 8.1 Schematic illustration of various ways of weakly orienting membrane proteins reconstituted in membrane-mimetic media. (A) Alignment by the paramagnetic tag (detergent resistant). (B) Alignment by the strained polyacrylamide gel (detergent resistant). (C) Alignment by DNA-based liquid crystals (detergent resistant). (D) Alignment by the Pf1 liquid crystal (not detergent resistant; must use lipid nanodiscs).

Liquid crystals have delicate phase transitions and usually disintegrate under extreme sample conditions, such as high temperature, low pH, and the presence of surfactants. The advantage of polyacrylamide gels is obvious because chemically cross-linked polymers can withstand very harsh sample conditions as long as they are properly hydrated. The SAG method has been used to weakly align membrane proteins in both detergent micelles[15,16,19,20] and lipid–detergent bicelles.[18] The idea of the SAG method is that the pores of the randomly cross-linked gel matrix are on average isotropic, and that straining the gel in one direction, *e.g.*, radially, can generate anisotropic pores and thus induce marginal alignment of the protein inside the pores (Figure 8.1B). This idea can be implemented in two ways. In one method, a cylinder-shaped polyacrylamide gel is first casted with a radius larger than that of a 5 mm Shigemi NMR tube, followed by dehydration and shrinking of the gel. The much-reduced gel is then placed in the 5 mm Shigemi tube preloaded with protein sample solution. As the protein sample soaks into the gel, the gel will expand to regain the original cylindrical dimensions, except that it is radially constrained by the inner diameter of the NMR tube. As a result, the gel is radially compressed, generating a distribution of anisotropic pores with the long axis aligned with the NMR tube and magnetic field. In another method, the original gel is partially dehydrated and soaked in the protein sample solution for protein loading. The fully hydrated gel with an 8 mm diameter is then squeezed into the narrower, open-ended NMR tube (5 mm) using a funnel-like device (commercially available at New Era NMR Inc.).[30] Application of the SAG method has been exemplified by the structural studies of the pentameric phospholamban in dodecylphosphocholine (DPC) micelles,[19] the tetrameric influenza M2 channel in DH_6PC micelles,[20] the DsbB disulfide exchange protein in DPC micelles,[15] and the DAGK in DPC micelles.[16]

Although the SAG method seems robust and insensitive to the surfactants used for membrane protein reconstitution, it has serious shortcomings. Since the polyacrylamide matrix is randomly cross-linked,[31] the pore size is highly inhomogeneous with only a fraction of the pores being large enough to afford free tumbling of membrane protein complexes, and thus the protein concentration (especially for membrane proteins complexed with large micelles or bicelles) in the gel achievable by soaking is often too low to generate strong signals. Further, the inhomogeneous pore size means inhomogeneous alignment and dipolar couplings. Both consequences of the inhomogeneous pore size above result in lower quality RDC measurements. While measurements of ^{15}H–^{1}H RDCs using 2D experiments are still feasible even for SAG samples with low protein concentrations (0.1–0.3 mM), other RDCs that require triple resonance experiments are very challenging to obtain.

8.2.2 Collagen Gel

Aligned hydrogels can also be made non-mechanically, and this was achieved by exploiting the temperature dependent polymerization of type I collagen.[32,33]

Monomers of fibrillar collagens have a triple-helical structure of ~1.5 nm diameter and 300 nm length, and they self-assemble to produce tightly packed periodic fibrils.[34] The high aspect ratio of the monomeric collagen rods yields high diamagnetic anisotropy, and thus anisotropic collagen gel can be made by thermally inducing polymerization in a strong magnetic field.[32] The application of the aligned collagen gel in RDC measurement was demonstrated by Ma *et al.* using the glutamine-binding protein (GlnBP) and was shown to be resistant to 100 mM DPC.[33] In this study, monomeric collagen rods of ~1.5 nm diameter were made to have a uniform length of 300 nm by cleaving the collagen fibril with interstitial collagenase, MMP-1.[35] The collagen monomer was first mixed with protein at low temperature (4 °C) to prevent polymerization. The mixture was put into an NMR tube and placed in a high field spectrometer. To achieve initial alignment of the collagen monomer in the magnetic field, the temperature was kept at 4 °C for 3 h and subsequently increased to 25 °C at a rate of 1 °C/10 min. The temperature was then further elevated to 37 °C at a rate of 1 °C/15 min for polymerization. The quadrupolar splitting of the ^{2}H NMR signal of the solvent could be observed when the temperature reached 32 °C. This splitting stabilized in two hours after the temperature was increased to 37 °C, indicating stable formation of the anisotropic collagen gel. In a collagen gel made with 13 mg mL^{-1} collagen, the GlnBP could be aligned to achieve a $^1D_{NH}$ of about ±10 Hz. Although application to membrane proteins has yet to be demonstrated, the collagen gels showed good detergent tolerance. For example, even the low-percentage collagen gels (1.4 mg mL^{-1}) were still stable after being soaked in a 100 mM DPC solution for several days (evaluated by the ^{2}H splitting that could still be observed), suggesting that it is a viable option for RDC measurements of membrane proteins.

8.2.3 DNA Nanotubes

DNA-based liquid crystals were developed to address the technical issues of SAG. DNA origami technology can be used for the design and construction of particles of various shapes[36,37] and, by virtue of being built from DNA, the particles are resistant to detergents. The first demonstration of this approach is the construction of a DNA nanotube that mimics the filamentous phage Pf1 (illustrated in Figure 8.1C). Pf1 phages are rod-like particles with a 6.5 nm diameter and a 2 μm length.[38] The liquid crystal formed by Pf1 is often the number one option for alignment of soluble proteins. The structural rigidity and negative surface charge density[39] of Pf1 phage particles allow them to form a stable liquid crystal at concentrations as low as 12 mg mL^{-1}.[23] Unfortunately, Pf1 is also not compatible with detergents. At 20 mg mL^{-1}, Pf1 is not liquid-crystalline at modest concentrations of the detergent, *e.g.*, ~50 mM DPC (unpublished results from my laboratory). Hence, a six-helix bundle DNA-nanotube architecture was designed using the scaffolded DNA origami method[40] to mimic a Pf1 particle.[41] The design resembles a parallel array of six double helices in which the adjacent double

helices are held together by Holliday junction crossovers. Using an M13-derived single-stranded circle of DNA containing 7308 bases as a "scaffold", 168 "staple" DNA oligos with a length of 42 bases were designed to form base pairing with three separate 14-base regions of the scaffold, folding the scaffold into a six-helix bundle nanotube of 0.4 μm length. To achieve nanotubes of 0.8 μm length, two types of 0.4 μm monomers were designed to specifically dimerize in a head-to-tail fashion.

The fabricated DNA nanotubes can form stable liquid crystals at a concentration of $\sim$25 mg mL^{-1}. The DNA nanotubes were tested for weak alignment of the transmembrane (TM) domain (residues 7–39) of the ζ–ζ chain of the TCR/CD3 complex reconstituted in mixed DPC/SDS micelles. The measured ^{1}H–^{15}N and ^{1}H$_{\alpha}$–^{13}C$_{\alpha}$ RDCs agree very well with the known NMR structure of the ζ–ζ TM domain,[42] with a correlation coefficient of the singular value decomposition (SVD) fit, R_{SVD}, of 0.98, or a free quality factor, Q_{free}, of 16%. The magnitude of the alignment tensor, D_a, at a 28 mg mL^{-1} nanotube concentration is 9.9 Hz (normalized to $^{1}D_{NH}$), which is ideal for RDC measurement and structure calculations. Unlike the Pf1 particles that align parallel to the applied magnetic field,[43] the six-helix bundle DNA-nanotube aligns perpendicular to the magnetic field because the diamagnetic DNA bases have the lowest energy when the field is parallel to the plane of the bases.[44]

8.2.4 G-tetrad Liquid Crystals

Although the DNA nanotube liquid crystal can display performance as good as Pf1 even in the presence of a strong detergent, it is very expensive to produce and thus cannot be easily commercialized. Hence, other forms of DNA-based liquid crystals that are more readily available have been explored. Lorieau *et al.* found that one suitable liquid crystal consists simply of the dinucleotide 2′-deoxyguanylyl-(3′,5′)-2′-deoxyguanosine (d(GpG)).[44] It is well known that guanosine mono-, di-, or larger oligonucleotides can form G-tetrad structures, where hydrogen bonds link four G bases in a C_4-symmetric planar arrangement, with cations on the C_4 axis coordinating the C6 carbonyl groups of G. Stacked columns of G-tetramers have a diameter of $\sim$2.5 nm (*vs.* 6.5 nm for Pf1) and, like the DNA nanotubes, are aligned perpendicular to the external magnetic field. At $\sim$25 mg mL^{-1} and a saturating amount of K^+ cations ($\gg$20 mM), d(GpG) can form a stable hexagonal liquid crystal in the presence of 100 mM DPC.[44] The d(GpG) liquid crystal was used to weakly align the hemagglutinin fusion peptide (HAfp) solubilized in DPC micelles. At 28 mg mL^{-1} of d(GpG), a D_a (normalized to $^{1}D_{NH}$) of $\sim$13 Hz was achieved for the peptide–micelle complex.[44]

8.2.5 Pinacyanol Acetate Liquid Crystals

Regions of membrane proteins or domains near the edge of the lipid bilayer often contain charged amino acids, and these residues could adversely

interact with charged alignment media, leading to slow rotational diffusion. Both DNA nanotubes and the G-tetrad are negatively charged, precluding their application to highly positively charged membrane proteins. It was later found that the liquid crystal formed by the dye pinacyanol acetate[45] can resist 100 mM DPC.[46] Since DPC is generally considered a strong detergent, the result suggests that the pinacyanol acetate (PNA) liquid crystal can resist most of the detergents used for membrane protein studies. Importantly, the PNA is positively charged and complement well the negatively charged nucleotide based liquid crystals. The PNA liquid crystal was demonstrated to marginally align the influenza hemagglutinin fusion peptide (HAfp) reconstituted in DPC micelles. In liquid crystals with $\sim$7.5 mg mL^{-1} PNA, a D_a (normalized to $^1D_{NH}$) of $-$11.9 Hz could be achieved.[46] Moreover, the alignment tensor is highly orthogonal to that in the K-d(GpG) liquid crystal, with a tensor product of $-$0.165. Hence, the PNA offers not only another alignment medium option for sample compatibility, but also orthogonal RDC data to resolve RDC orientational degeneracy during structure determination.

8.2.6 The Use of Lipid Nanodiscs for Membrane Protein Reconstitution

An alternative approach to using detergent-resistant alignment media is to reconstitute membrane proteins in lipid nanodiscs, which does not involve detergents in their final form. Lipid nanodiscs are patches of lipid bilayers enclosed by membrane scaffold proteins (MSPs), which are truncated forms of human serum apolipoprotein A1 with a hydrophobic surface interacting with lipids and a hydrophilic surface exposed to a solvent.[47,48] The commonly used nanodiscs are 10–15 nm in diameter and have a molecular weight (M.W.) ranging from 150 to 200 kDa. The large size of nanodiscs has, in the past, discouraged NMR spectroscopists but they have been revisited in the last decade owing to much improved NMR technology and sensitivity. It has been shown that medium sized membrane proteins such as the human voltage-dependent anion channel (VDAC) and the rat neurotensin receptor 1 (NTR1) in nanodiscs of $\sim$10 nm size can generate good quality two-dimensional NMR spectra under the conditions of protein deuteration, TROSY, high temperature (45 °C) and high magnetic field.[49,50] The slow rotational diffusion rate ($\tau_c \sim 50$ ns for a 10 nm nanodisc), however, precludes more in-depth NMR studies such as backbone resonance assignment and NOE measurements that necessitate the use of 3D/4D experiments. To address the problem of large τ_c, smaller nanodiscs with diameters ranging from 6 to 8 nm have been developed by engineering shorter truncated ApoA-I variants.[51,52] For example, the MSP construct with the H5 helix deleted, designated MSPΔH5, assembles nanodiscs of $\sim$8 nm diameter with a τ_c of 34 ns. The relatively small membrane protein OmpX (148aa) reconstituted in the MSPΔH5 nanodisc exhibited relaxation properties that allowed recording of triple-resonance spectra and >90% assignment of backbone resonances.[51] The obvious advantage of the nanodisc system is that there is

no detergent in the final sample, thus enabling the use of regular alignment media such as Pf1 (Figure 8.1D). Indeed, weak alignment of OmpX in the MSPΔH5 nanodisc has been achieved with 10 mg mL^{-1} Pf1, resulting in NH RDCs ranging from −19.8 to 23.7 Hz.[53]

8.3 RDC Measurements

Membrane proteins usually tumble slowly in solution due to the added mass of detergent micelles, lipid–detergent bicelles, or lipid nanodiscs. With τ_c on average >25 ns, the proteins need to be deuterated, at least partially, for transverse relaxation optimization of ^{15}N and ^{13}C and for reducing adverse ^{1}H–^{1}H dipolar interactions in the aligned sample. Hence, large RDCs such as those of Cα–Hα or Cβ–Hβ are generally not accessible for membrane proteins. Three types of backbone RDCs however can be measured to reasonable accuracy using ^{15}N, ^{13}C and ∼85% ^{2}H labeled protein, the type of labeling scheme typically used for triple resonance experiments; they are coupling constants for the backbone chemical bonds H_N–N, C′–C_α, and C′–N.

The $^{1}H_N$–^{15}N couplings can be measured using the *J*-scaled TROSY-HNCO experiment to exploit the favorable relaxation properties of the TROSY transitions.[54–56] In this experiment, two interleaved spectra are recorded, the regular TROSY-HNCO and a modified TROSY-HNCO with J_{NH} evolution during the ^{15}N chemical shift evolution scaled down, for example, to zero. Although the *J*-scaled experiment reduces coupling size and thus increases uncertainty in RDC measurement, it circumvents the rapid relaxation of the anti-TROSY component which cannot be measured at all for most slow tumbling proteins.

Since the ^{13}C′–$^{13}C^{\alpha}$ and ^{13}C′–^{15}N scalar coupling constants are much smaller than that of $^{1}H_N$–^{15}N, complete separation of the doublet required for coupling constant measurement would involve long evolution of the $^{13}C^{\alpha}$ and ^{15}N transverse magnetization. Therefore, the quantitative *J* correlation method is better suited for measuring these small coupling constants. The ^{13}C′–$^{13}C^{\alpha}$ coupling is measured using the 3D TROSY-HNCA experiment with quantitative $J_{C\alpha C'}$ modulations of 0 and 28 ms.[57] The ^{13}C′–^{15}N coupling is measured using the 3D TROSY-HNCO experiment with quantitative $J_{NC'}$ modulations of 33 and 66 ms.[58] The quantitative *J* correlation method can also be implemented for measuring $^{1}H_N$–^{15}N coupling constants when the protein is perdeuterated. In this case, active J_{NH} dephasing can be applied to the ^{1}H transverse magnetization during the first INEPT of TROSY-HSQC. The coupling constant can be extracted from two interleaved spectra recorded with J_{NH} evolutions of 5.35 and 10.7 ms, respectively.[59]

8.4 Use of RDCs in Structural Characterization of Membrane Proteins

Probably the biggest advantage of RDC restraints is that they are completely quantitative and unambiguous. Being quantitative means the one-bond RDC

value has a clear mathematical relation to the orientation of the chemical bond, although serious orientation degeneracy exists. RDC values are unambiguous in terms of assignment because they are measured based on the sequence-specific assignment of backbone resonances, which is usually very reliable in modern protein NMR spectroscopy. Therefore, RDC values can be used as numerical data for structure determination, like diffraction in X-ray crystallography. A still active area of research is finding the most effective way to use RDCs in structure determination. The major shortcoming of RDCs is that they do not provide translational information of the corresponding chemical bonds and thus need to be used in combination with distance restraints for *de novo* structure determination.

8.4.1 Restrained Molecular Dynamics and Simulated Annealing

The restrained molecular dynamics (rMD) algorithm combined with the simulated annealing (SA) protocol, implemented in XPLOR-NIH,[60] has been the standard method for NMR-based structure calculations. The rMD involves numerically solving Newton's equations of motion for a polymer system in which the total potential energy is the sum of physical potentials (*e.g.*, chemical bonds, angles, van der Waals, *etc.*) and pseudopotentials from experimental restraints (*e.g.*, interatomic distances, dihedral angles, bond orientations, *etc.*).[61,62] For macromolecules, the refinement energy landscape becomes very complicated, posing serious problems of local minima. Therefore, the rMD calculation is done in combination with simulated annealing (heating the system, followed by gradual cooling), an effective protocol for "jumping" out of false local minima.[63,64] In principle, this method can be used to minimize variable target functions of any type and is thus readily applicable to refining structures against RDCs.

Protocols for incorporating RDCs in structure calculations are the same for membrane proteins as they are for other soluble proteins. A problem worth noting is that membrane proteins often have fewer NOE-derived restraints due to a number of technical issues associated with NMR data analysis. (1) Membrane proteins need to be solubilized in detergent micelles or lipid/detergent bicelles, and how these membrane-mimetic surfactants assemble around a protein could depend on the protein, the type of surfactants, or both. Heterogeneous association of lipids and/or detergents often result in heterogeneous line broadening of the protein resonances. Furthermore, the presence of very high concentrations of the detergent requires methods to suppress NMR signals arising from the detergent, and this can be challenging for experiments such as ^{13}C-edited NOESY if a non-deuterated lipid/detergent is used. (2) In general, membrane proteins contain proportionally many more methyl-bearing amino acids than water-soluble proteins, resulting in a more crowded methyl spectrum and greater methyl chemical shift ambiguity. The above issues limit the amount and accuracy of long-range NOEs that can be assigned. Hence, structural studies

of membrane proteins involve collecting other restraints such as PREs and/or RDCs to complement NOEs. Typically, the RDCs are applied in the stage of structure refinement after the global fold of the protein is known from either NOEs/PREs or homology modeling. In the context of a correct global fold, RDCs would be most effective in adjusting the relative orientation of secondary segments.

Refinement of RDCs in structure calculations typically requires preliminary assessment of D_a and R_h of the alignment tensor based on experimental RDC values. Estimation of D_a and R_h can be done using the RDC histogram approach if measured RDCs include sufficiently broad orientation sampling,[65] but such condition is often hard to achieve for membrane proteins. With the requirement for bicelles or micelles, membrane proteins, even small transmembrane domains, have short T_2 and need to be deuterated. For ^{15}N, ^{13}C, and deuterated protein, three backbone RDCs that can be measured to reasonable accuracy are those of H_N–N, C′–C_α, and C′–N[66–68] and these are often insufficient to generate a smooth histogram. Bryce and Bax have developed an extended histogram method (EHM) to smoothen the RDC histogram by exploiting the correlated nature of RDCs for structural elements within the planar peptide unit.[69] More accurate starting values of D_a and R_h would render RDC refinement more effective. For detailed structure refinement protocols in XPLOR-NIH, please see Chapter 7.

8.4.2 RDC-based Molecular Fragment Replacement

An alternative way to use RDCs for structural characterization is to exhaustively search the protein database for structural fragments that best fit experimental data, commonly known as the molecular fragment replacement (MFR) method. The MFR method was first used in crystallography for building molecular fragments into low resolution crystallographic density[70] and was subsequently applied in NMR to fragments that agree with RDCs[71] and other NMR data such as chemical shifts.[72,73] Although in principle the MFR approach limits the conformational space to what has already been observed, in practice this approach demonstrated to be very effective because (1) the Protein Data Bank is so large and diverse that its content is an excellent representation of the conformational space of proteins and nucleic acids in nature and (2) the method greatly reduces the search space such that it is computationally affordable. Furthermore, the structure database is expanding at a rapid pace and thus the MFR approach would only become more powerful with time.

The first proof-of-principle study of RDC-based MFR showed that, with about four RDCs per residue, it is possible to determine the backbone structure of ubiquitin using molecular fragments that fit to RDCs.[74] This study suggests that if a protein is mostly structured and overall rigid, such as ubiquitin, RDC-based MFR can be used to derive the tertiary backbone structure even without using distance restraints. For the majority of the proteins that have flexible loops or internal dynamics, however, distance

restraints are still needed as RDCs do not provide translational information. Fragment searching that combines chemical shifts and RDCs has also been implemented in the CS-Rosetta structure modeling software and demonstrated to be effective in solving water-soluble protein structures.[75,76] As an example of application to membrane proteins, the RDC-based MFR study on the mitochondrial uncoupling protein 2 (UCP2) is described below.[77]

UCP2 belongs to a family of relatively small transporters ($\sim$30 kDa) in the inner membrane of mitochondria known as mitochondrial carriers. The canonical function of mitochondrial carriers is transporting negatively charged metabolites, although the primary function of UCPs is translocating protons by flipping ionized fatty acids across the membrane.[78,79] Mitochondrial carriers have been extremely difficult targets for structure determination by crystallography and cryo-EM due to their small size and dynamic nature,[80] hence the need for structural examination by NMR. The known transporter structures in the database show that the transmembrane (TM) segments often adopt unusual helical features such as kinks, bends, and irregular helical turns that could be important for tolerating conformational switches.[81] These features, which are often difficult to determine using local NOE restraints, can be identified by exhaustively searching for structured fragments in the protein structure database that agree well with experimental RDCs.

In the case of UCP2, a large fragment library containing 320 000 7-residue fragments from 1514 protein structures was constructed, and from the library, a set of candidate fragments with good RDC fitting ($Q_{\text{free}} < 25\%$) and the correct alignment tensor values were found for every possible 7-residue sequence of UCP2 that has sufficiently dense RDC data. For a particular 7-residue stretch of UCP2, if the structures of its best candidate fragments converge, then there is strong statistical confidence that the fragments represent a unique structural solution for this sequence stretch. Based on this principle, the candidate fragments were assigned to the protein sequence and this step is known as *fragment assignment* (Figure 8.2A). The next procedure was building longer structured segments using two operations: *end extension* and *gap filling*. End extension is extending the N- or C-terminal end of a structurally assigned segment along the protein sequence by searching for unused candidate fragments that overlap with the segment in backbone dihedral angles, and that provide the best Q_{free} for the final extended segment (Figure 8.2B). Similarly, gap filling is to fill gap regions (<4 residues) between two structurally assigned segments by searching for fragments that overlap in backbone dihedral angles with the two flanking segments and that provide good Q_{free} for the merged segment (Figure 8.2C). These two operations were repeated to assign as much structure as possible to the protein sequence. Although RDCs were used in the MFR method, the MFR algorithm can also include other data such as chemical shifts and local NOEs if they are available. Using this iterative procedure, 15 structured segments were assigned to the UCP2 sequence, of which a few indeed show bents or kinks.

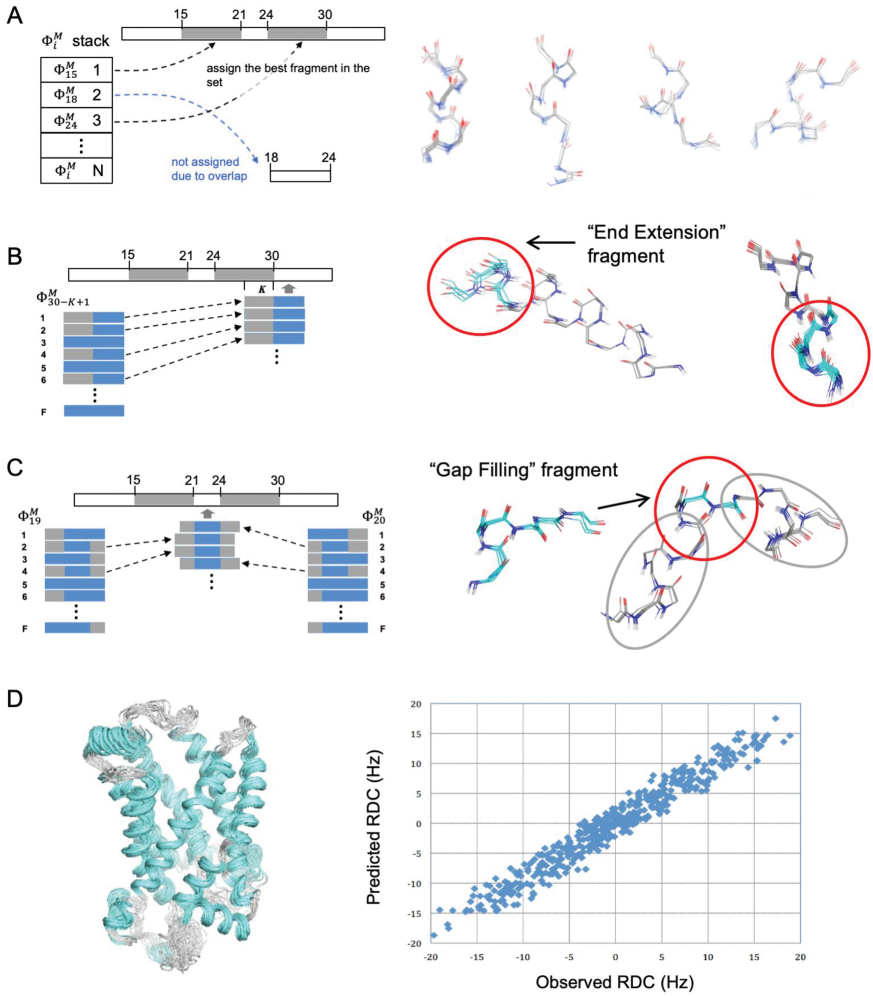

Figure 8.2 Conceptual illustration of the operations involved in RDC-based molecular fragment searching and structural segment building. (A) Fragment assignment. (B) End extension. (C) Gap filling. Details are described in the text. (D) An ensemble of 15 low-energy structures calculated with 15 structured segments from RDC-based molecular fragment searching, PRE restraints from four spin label positions, and all RDCs. The right panel shows the overall agreement between RDCs and the final calculated structure. Reproduced from ref. 77 with permission from Springer Nature, Copyright 2011.

As mentioned above, RDCs do not provide translational information of the structured segments and thus need to be used in conjunction with distance restraints to solve the protein tertiary structure. For UCP2, semiquantitative distance restraints derived from paramagnetic relaxation enhancement (PRE) measurements[14] were obtained. The paramagnetic label used for PRE

measurement was the nitroxide spin label in *S*-(2,2,5,5-tetramethyl-2,5-dihydro-1*H*-pyrrol-3-yl)methyl methanesulfonothioate (MTSL), which was covalently attached at a single cysteine position. Four samples were produced, each with MTSL attached to Cys68, Cys105, Cys202 or Cys255, and these samples collectively provided ~450 PRE distance restraints. Finally, to calculate the tertiary structure, the 15 structured segments derived from MFR were treated as rigid bodies, *e.g.*, grouping the backbone Cα atoms in the XPLOR-NIH program,[60] while applying the PRE and RDC restraints (Figure 8.2D). During the rMD/SA calculation, the MFR segments make up most of the local structure of the protein, and the PRE and RDC measurements provided spatial and orientational restraints, respectively, for these structured segments.

8.4.3 Potential Application to Symmetric Oligomers

As mentioned above in the introduction, one of the most successful NMR applications to membrane biology has been on transmembrane domains, usually single transmembrane helices (TMHs) of type I/II membrane proteins that remain largely inaccessible to crystallography or cryo-EM. Single TMHs can be interesting because they often form homo-oligomers with C_n symmetry. Determining the oligomeric TMH structures is important for revealing the assembly interface residues to inform functional mutagenesis and many transmembrane receptors bear disease mutations within the TMH.

For simple molecules with C_3 or higher symmetry, $R_h = 0$ and the alignment tensor is axially symmetric, as has been shown for benzene-like small molecules.[82] Hence, for TMH homotrimers or higher oligomers, their alignment tensors are thought to be axially symmetric as well (Figure 8.3A). This would be very convenient because the RDC of a bond vector would have a simple dependence of $3\cos^2\theta - 1$, where θ is the angle between the bond vector and the symmetry axis of the TMH oligomer. Knowing the precise orientation of the bond vectors relative to the symmetry axis might allow for rapid determination of the oligomer structure without measuring intermolecular NOEs by simply optimizing the helix–helix van der Waals interaction. The situation is, however, somewhat different in practice as RDCs obtained for the tetrameric TMH of the influenza M2 and the pentameric TMH of phospholamban deviate substantially from an axially symmetric tensor.[19,20] Both TMD oligomers were reconstituted in phosphocholine detergent and appeared stable enough to migrate in SDS-PAGE as a single oligomeric species without any crosslinking.[19,20,83] One possibility is that although the TMDs remain oligomeric in detergent micelles, they are not held together in a completely rigid manner. Since alignment can be introduced on the nanosecond time scale, even the highly transient deviation from symmetry could contribute significantly to the average alignment tensor. Moreover, a more recent theoretical analysis of partial alignment and molecular symmetry argued that an axially symmetric alignment tensor

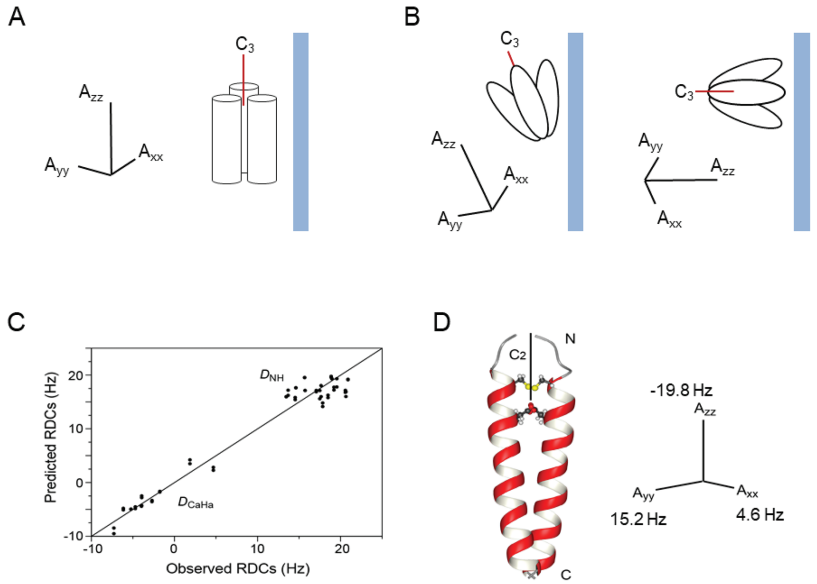

Figure 8.3 Application of RDCs to transmembrane helices that form symmetric oligomers. (A) Illustration of an axially symmetric tensor for a hypothetical transmembrane helix (TMH) trimer with one dominant interaction with the alignment medium that averages around the axis of molecular symmetry. (B) Another hypothetical TMH trimer structure with two major modes of alignment interactions, resulting in two different alignment tensors that may not average to an axially symmetric tensor. (C) Analysis of RDCs measured for the detergent-reconstituted TMH dimer of the ζ chain of the T-cell receptor complex, weakly aligned in 28 mg mL^{-1} DNA nanotube. Correlation between the observed backbone RDCs (normalized to D_{NH}) and RDCs predicted for the known NMR structure of ζ–ζ TMH (PDB entry 2HAC), using an alignment tensor obtained from the SVD fit. The correlation coefficient R_{SVD} is 0.98 and Q_{free} is 16%. (D) Principal axes of the alignment tensor relative to 2HAC: $A_{zz} = -19.8$ Hz, $A_{yy} = 15.2$ Hz, $A_{xx} = 4.6$ Hz, $D_a^{NH} = -9.9$ Hz, and rhombicity, $R_h = 0.357$. The solid line in the ribbon structure represents the axis of C_2 rotational symmetry. (C) and (D) Reproduced from ref. 41 with permission from PNAS, Copyright (2007) National Academy of Sciences, U.S.A.

is applicable when there is only one dominant interaction (Figure 8.3A) between the oligomer and the alignment medium responsible for rotational averaging around the axis of molecular symmetry.[84] When there are more than one major interactions for the same symmetry orientation, as illustrated in Figure 8.3B, the averaged alignment tensor may no longer be axially symmetric.

Despite the above plausible explanations for tetrameric or pentameric TMHs not showing an axially symmetric alignment tensor, it is important to emphasize that the amount of RDC data available for oligomeric TMHs is still very limited and more RDC data need to be acquired for various TMH

oligomers that have been demonstrated to be highly stable. Another RDC data set worth mentioning is that of the TMH of the ζ chain of the T-cell receptor complex.[41] This TMH forms a strong homodimer stabilized by an inter-chain disulfide bond.[85] For dimers with C_2 symmetry, the principal axis of the alignment tensor is predicted to be parallel to the C_2 axis although $R_h \neq 0$. Backbone ^1H–^{15}N and $^1H_\alpha$–$^{13}C_\alpha$ RDCs were measured for the TMH dimer of the ζ–ζ chain weakly aligned in DNA nanotube liquid crystals.[41] The measured RDCs fitted very well to the NMR structure ($R_{SVD} = 0.98$, $Q_{free} = 0.16$) and determined an alignment tensor with $D_a = 9.9$ Hz (normalized to D_{NH}) and $R_h = 0.357$ (Figure 8.3C). In this case, the axis of C_2 rotational symmetry of the dimer is parallel to the largest principal axis, A_{zz}, of the alignment tensor (Figure 8.3D).

8.5 Challenges and Future Perspectives

The basic protocols of protein NMR spectroscopy for membrane proteins are no different than those of soluble proteins. The challenges of membrane protein NMR are generally associated with low quality NMR data, which could be attributed to many factors such as the heterogeneous chemical environment caused by detergent/lipid partition, added molecular weight due to membrane mimetic media, as well as the intrinsic conformational dynamics of membrane proteins. Hence, structural characterization of membrane proteins by NMR is usually compromised by sparse experimental restraints. RDCs encode orientation information completely orthogonal to NOE- and PRE-derived distance restraints, and thus could be very powerful in compensating for the lack of experimental data. The reason for RDCs not being used more often for membrane proteins is still the technical inconveniences associated with measuring and analyzing RDCs, and thus further improvements on these fronts would greatly enhance their application.

First, although a large variety of experiments have been published for measuring RDCs, preparation of an optimally aligned sample often requires repeated testing of different alignment media and buffer conditions, which consumes a large amount of protein samples. Since membrane protein samples are generally expensive and time-consuming to make, researchers are often not willing to allocate a large amount of resources and efforts to collect RDCs unless they are the only source of structural information. Therefore, development of a highly robust and inert alignment medium for membrane protein samples would drastically expand the RDC application for membrane proteins. Second, refinement of structures against RDCs remains a precarious issue, and in many cases one cannot be certain that RDC refinement with rMD/SA protocols actually improves the accuracy of the structure because the refinement program can tweak the bonds to satisfy RDCs depending on the force constants applied. For example, the slow tumbling membrane proteins typically only allow the measurement of NH RDCs. Given the orientation degeneracy of RDCs, applying only NH RDCs

could run into the risk of fine-tuning the bond vector orientation locally that might not improve the global orientation accuracy of the secondary segments. Hence, further improvement in computational methods that combine RDCs with learning-based structure prediction methods, such as AlphaFold[86,87] and Rosetta,[76] would maximize the utility of RDCs in structure determination.

References

1. M. E. Call and J. J. Chou, A view into the blind spot: solution NMR provides new insights into signal transduction across the lipid bilayer, *Structure*, 2010, **18**, 1559–1569.
2. Z. L. Dong, J. Lin, B. Zhang, Y. Zhu, N. Li, S. Xie, Y. Wang, N. Gao and Z. Huang, Structural basis of assembly of the human T cell receptor-CD3 complex, *Nature*, 2019, **573**, 546–552.
3. M. E. Call and K. W. Wucherpfennig, Common themes in the assembly and architecture of activating immune receptors, *Nat. Rev. Immunol.*, 2007, **7**, 841–850.
4. M. E. Call, K. W. Wucherpfennig and J. J. Chou, The structural basis for intramembrane assembly of an activating immunoreceptor complex, *Nat. Immunol.*, 2010, **11**, 1023–1029.
5. E. V. Bocharov, *et al.*, Spatial structure of the dimeric transmembrane domain of the growth factor receptor ErbB2 presumably corresponding to the receptor active state, *J. Biol. Chem.*, 2008, **283**, 6950–6956.
6. N. F. Endres, *et al.*, Conformational coupling across the plasma membrane in activation of the EGF receptor, *Cell*, 2013, **152**, 543–556.
7. J. Dev, *et al.*, Structural basis for membrane anchoring of HIV-1 envelope spike, *Science*, 2016, **353**, 172–175.
8. Q. Fu, *et al.*, Structural Basis and Functional Role of Intramembrane Trimerization of the Fas/CD95 Death Receptor, *Mol. Cell*, 2016, **61**, 602–613.
9. L. Pan, *et al.*, Higher-Order Clustering of the Transmembrane Anchor of DR5 Drives Signaling, *Cell*, 2019, **176**, 1477–1489 e1414.
10. T. L. Lau, C. Kim, M. H. Ginsberg and T. S. Ulmer, The structure of the integrin alphaIIbbeta3 transmembrane complex explains integrin transmembrane signalling, *EMBO J.*, 2009, **28**, 1351–1361.
11. J. Zhu, *et al.*, Structure of a complete integrin ectodomain in a physiologic resting state and activation and deactivation by applied forces, *Mol. Cell*, 2008, **32**, 849–861.
12. B. OuYang and J. J. Chou, The minimalist architectures of viroporins and their therapeutic implications, *Biochem. Biophys. Acta*, 2014, **1838**, 1058–1067.
13. C. Xu, *et al.*, Regulation of T cell receptor activation by dynamic membrane binding of the CD3epsilon cytoplasmic tyrosine-based motif, *Cell*, 2008, **135**, 702–713.
14. J. L. Battiste and G. Wagner, Utilization of site-directed spin labeling and high-resolution heteronuclear nuclear magnetic resonance for global

fold determination of large proteins with limited nuclear overhauser effect data, *Biochemistry*, 2000, **39**, 5355–5365.
15. Y. Zhou, *et al.*, NMR solution structure of the integral membrane enzyme DsbB: functional insights into DsbB-catalyzed disulfide bond formation, *Mol. Cell*, 2008, **31**, 896–908.
16. W. D. Van Horn, *et al.*, Solution nuclear magnetic resonance structure of membrane-integral diacylglycerol kinase, *Science*, 2009, **324**, 1726–1729.
17. B. Liang, J. H. Bushweller and L. K. Tamm, Site-directed parallel spin-labeling and paramagnetic relaxation enhancement in structure determination of membrane proteins by solution NMR spectroscopy, *J. Am. Chem. Soc.*, 2006, **128**, 4389–4397.
18. J. J. Chou, J. D. Kaufman, S. J. Stahl, P. T. Wingfield and A. Bax, Micelle-induced curvature in a water-insoluble HIV-1 Env peptide revealed by NMR dipolar coupling measurement in stretched polyacrylamide gel, *J. Am. Chem. Soc.*, 2002, **124**, 2450–2451.
19. K. Oxenoid and J. J. Chou, The structure of phospholamban pentamer reveals a channel-like architecture in membranes, *Proc. Natl. Acad. Sci. U. S. A.*, 2005, **102**, 10870–10875.
20. J. R. Schnell and J. J. Chou, Structure and mechanism of the M2 proton channel of influenza A virus, *Nature*, 2008, **451**, 591–595.
21. A. Bax, G. Kontaxis and N. Tjandra, Dipolar couplings in macromolecular structure determination, *Methods in Enzymology*, 2001, vol. 339, pp. 127–174.
22. N. Tjandra and A. Bax, Direct measurement of distances and angles in biomolecules by NMR in a dilute liquid crystalline medium, *Science*, 1997, **278**, 1111–1114.
23. M. R. Hansen, L. Mueller and A. Pardi, Tunable alignment of macromolecules by filamentous phage yields dipolar coupling interactions, *Nat. Struct. Biol.*, 1998, **5**, 1065–1074.
24. G. M. Clore, M. R. Starich and A. M. Gronenborn, Measurement of residual dipolar couplings of macromolecules aligned in the nematic phase of a colloidal suspension of rod-shaped viruses, *J. Am. Chem. Soc.*, 1998, **120**, 10571–10572.
25. M. Rückert and G. Otting, Alignment of Biological Macromolecules in Novel Nonionic Liquid Crystalline Media for NMR Experiments, *J. Am. Chem. Soc.*, 2000, **122**, 7793–7797.
26. K. Fleming, D. Gray, S. Prasannan and S. Matthews, Cellulose crystallites: A new and robust liquid crystalline medium for the measurement of residual dipolar couplings, *J. Am. Chem. Soc.*, 2000, **122**, 5224–5225.
27. C. Ma and S. J. Opella, Lanthanide ions bind specifically to an added "EF-hand" and orient a membrane protein in micelles for solution NMR spectroscopy, *J. Magn. Reson.*, 2000, **146**, 381–384.
28. R. Tycko, F. J. Blanco and Y. Ishii, Alignment of biopolymers in strained gels: A new way to create detectable dipole–dipole couplings in high-resolution biomolecular NMR, *J. Am. Chem. Soc.*, 2000, **122**, 9340–9341.

29. H. J. Sass, G. Musco, S. J. Stahl, P. T. Wingfield and S. Grzesiek, Solution NMR of proteins within polyacrylamide gels: Diffusional properties and residual alignment by mechanical stress or embedding of oriented purple membranes, *J. Biomol. NMR*, 2000, **18**, 303–309.
30. J. J. Chou, S. Gaemers, B. Howder, J. M. Louis and A. Bax, A simple apparatus for generating stretched polyacrylamide gels, yielding uniform alignment of proteins and detergent micelles, *J. Biomol. NMR*, 2001, **21**, 377–382.
31. X. Z. Zhang, Y. Y. Yang, T. S. Chung and K. X. Ma, Preparation and characterization of fast response macroporous poly(*N*-isopropylacrylamide) hydrogels, *Langmuir*, 2001, **17**, 6094–6099.
32. J. Torbet and M. C. Ronziere, Magnetic alignment of collagen during self-assembly, *Biochem. J.*, 1984, **219**, 1057–1059.
33. J. Ma, G. I. Goldberg and N. Tjandra, Weak alignment of biomacromolecules in collagen gels: an alternative way to yield residual dipolar couplings for NMR measurements, *J. Am. Chem. Soc.*, 2008, **130**, 16148–16149.
34. K. E. Kadler, D. F. Holmes, J. A. Trotter and J. A. Chapman, Collagen fibril formation, *Biochem. J.*, 1996, **316**(Pt 1), 1–11.
35. S. Saffarian, I. E. Collier, B. L. Marmer, E. L. Elson and G. Goldberg, Interstitial collagenase is a Brownian ratchet driven by proteolysis of collagen, *Science*, 2004, **306**, 108–111.
36. N. C. Seeman, DNA in a material world, *Nature*, 2003, **421**, 427–431.
37. N. C. Seeman, Structural DNA nanotechnology: an overview, *Methods Mol. Biol.*, 2005, **303**, 143–166.
38. D. A. Marvin, Filamentous phage structure, infection and assembly, *Curr. Opin. Struct. Biol.*, 1998, **8**, 150–158.
39. K. Zimmermann, H. Hagedorn, C. C. Heuck, M. Hinrichsen and H. Ludwig, The ionic properties of the filamentous bacteriophages Pf1 and fd, *J. Biol. Chem.*, 1986, **261**, 1653–1655.
40. P. W. Rothemund, Folding DNA to create nanoscale shapes and patterns, *Nature*, 2006, **440**, 297–302.
41. S. M. Douglas, J. J. Chou and W. M. Shih, From the cover: DNA-nanotube-induced alignment of membrane proteins for NMR, *Proc. Natl. Acad. Sci. U. S. A.*, 2007, **104**, 6644–6648.
42. M. E. Call, *et al.*, The Structure of the ζζ Transmembrane Dimer Reveals Features Essential for Its Assembly with the T Cell Receptor, *Cell*, 2006, **127**, 355–368.
43. J. Torbet and G. Maret, High-field magnetic birefringence study of the structure of rodlike phages Pf1 and fd in solution, *Biopolymers*, 1981, **20**, 2657–2669.
44. J. Lorieau, L. Yao and A. Bax, Liquid crystalline phase of G-tetrad DNA for NMR study of detergent-solubilized proteins, *J. Am. Chem. Soc.*, 2008, **130**, 7536–7537.
45. C. Rodriguez-Abreu, C. A. Torres and G. J. Tiddy, Chromonic liquid crystalline phases of pinacyanol acetate: characterization and use as

templates for the preparation of mesoporous silica nanofibers, *Langmuir*, 2011, **27**, 3067–3073.
46. P. Thiagarajan-Rosenkranz, A. W. Draney, S. T. Smrt and J. L. Lorieau, A Positively Charged Liquid Crystalline Medium for Measuring Residual Dipolar Couplings in Membrane Proteins by NMR, *J. Am. Chem. Soc.*, 2015, **137**, 11932–11934.
47. A. Nath, W. M. Atkins and S. G. Sligar, Applications of phospholipid bilayer nanodiscs in the study of membranes and membrane proteins, *Biochemistry*, 2007, **46**, 2059–2069.
48. A. Nath, Y. V. Grinkova, S. G. Sligar and W. M. Atkins, Ligand binding to cytochrome P450 3A4 in phospholipid bilayer nanodiscs: the effect of model membranes, *J. Biol. Chem.*, 2007, **282**, 28309–28320.
49. T. Raschle, *et al.*, Structural and Functional Characterization of the Integral Membrane Protein VDAC-1 in Lipid Bilayer Nanodiscs, *J. Am. Chem. Soc.*, 2009, **131**, 17777–17779.
50. M. L. Nasr, *et al.*, Covalently circularized nanodiscs for studying membrane proteins and viral entry, *Nat. Methods*, 2017, **14**, 49–52.
51. F. Hagn, M. Etzkorn, T. Raschle and G. Wagner, Optimized phospholipid bilayer nanodiscs facilitate high-resolution structure determination of membrane proteins, *J. Am. Chem. Soc.*, 2013, **135**, 1919–1925.
52. F. Hagn, M. L. Nasr and G. Wagner, Assembly of phospholipid nanodiscs of controlled size for structural studies of membrane proteins by NMR, *Nat. Protoc.*, 2018, **13**, 79–98.
53. S. Bibow, *et al.*, Measuring membrane protein bond orientations in nanodiscs *via* residual dipolar couplings, *Protein Sci.*, 2014, **23**, 851–856.
54. G. Kontaxis, G. Clore and A. Bax, Evaluation of cross-correlation effects and measurement of one-bond couplings in proteins with short transverse relaxation times, *J. Magn. Reson.*, 2000, **143**, 184–196.
55. D. Yang, R. A. Venters, G. A. Mueller, W. Y. Choy and L. E. Kay, TROSY-based HNCO pulse sequences for the measurement of ^{1}HN–^{15}N, ^{15}N–^{13}CO, ^{1}HN–^{13}CO, ^{13}CO–^{13}C$^{\alpha}$ and ^{1}HN–^{13}C$^{\alpha}$ dipolar couplings in ^{15}N, ^{13}C, ^{2}H-labeled proteins, *J. Biomol. NMR*, 1999, **14**, 333–343.
56. L. Arbogast, A. Majumdar and J. R. Tolman, HNCO-based measurement of one-bond amide ^{15}N–^{1}H couplings with optimized precision, *J. Biomol. NMR*, 2010, **46**, 175–189.
57. C. P. Jaroniec, T. S. Ulmer and A. Bax, Quantitative J correlation methods for the accurate measurement of ^{13}C′–^{13}C$^{\alpha}$ dipolar couplings in proteins, *J. Biomol. NMR*, 2004, **30**, 181–194.
58. J. J. Chou, F. Delaglio and A. Bax, Measurement of one-bond ^{15}N–^{13}C′ dipolar couplings in medium sized proteins, *J. Biomol. NMR*, 2000, **18**, 101–105.
59. N. C. Fitzkee and A. Bax, Facile measurement of ^{1}H–^{15}N residual dipolar couplings in larger perdeuterated proteins, *J. Biomol. NMR*, 2010, **48**, 65–70.
60. C. D. Schwieters, J. Kuszewski, N. Tjandra and G. M. Clore, The Xplor-NIH NMR molecular structure determination package, *J. Magn. Reson.*, 2002, **160**, 66–74.

61. R. Kaptein, E. R. P. Zuiderweg, R. M. Scheek, R. Boelens and W. F. Vangunsteren, A Protein-Structure From Nuclear Magnetic-Resonance Data – Lac Repressor Headpiece, *J. Mol. Biol.*, 1985, **182**, 179–182.
62. G. M. Clore, *et al.*, The 3-Dimensional Structure Of Alpha-1-Purothionin In Solution – Combined Use Of Nuclear-Magnetic-Resonance, Distance Geometry And Restrained Molecular-Dynamics, *EMBO J.*, 1986, **5**, 2729–2735.
63. G. M. Clore, A. T. Brunger, M. Karplus and A. M. Gronenborn, Application Of Molecular-Dynamics With Interproton Distance Restraints To 3-Dimensional Protein-Structure Determination – A Model Study Of Crambin, *J. Mol. Biol.*, 1986, **191**, 523–551.
64. M. Nilges, G. M. Clore and A. M. Gronenborn, Determination Of 3-Dimensional Structures Of Proteins From Interproton Distance Data By Hybrid Distance Geometry-Dynamical Simulated Annealing Calculations, *FEBS Lett.*, 1988, **229**, 317–324.
65. G. M. Clore, A. M. Gronenborn and A. Bax, A Robust Method for Determining the Magnitude of the Fully Asymmetric Alignment Tensor of Oriented Macromolecules in the Absence of Structural Information, *J. Magn. Reson.*, 1998, **133**, 216–221.
66. G. Kontaxis, G. Clore and A. Bax, Evaluation of cross-correlation effects and measurement of one-bond couplings in proteins with short transverse relaxation times, *J. Magn. Reson.*, 2000, **143**, 184–196.
67. J. J. Chou, F. Delaglio and A. Bax, Measurement of one-bond ^{15}N–$^{13}C'$ dipolar couplings in medium sized proteins, *J. Biomol. NMR*, 2000, **18**, 101–105.
68. C. P. Jaroniec, T. S. Ulmer and A. Bax, Quantitative J correlation methods for the accurate measurement of $^{13}C'$–$^{13}C^{\alpha}$ dipolar couplings in proteins, *J. Biomol. NMR*, 2004, **30**, 181–194.
69. D. L. Bryce and A. Bax, Application of correlated residual dipolar couplings to the determination of the molecular alignment tensor magnitude of oriented proteins and nucleic acids, *J. Biomol. NMR*, 2004, **28**, 273–287.
70. T. A. Jones and S. Thirup, Using Known Substructures In Protein Model-Building And Crystallography, *EMBO J.*, 1986, **5**, 819–822.
71. F. Delaglio, G. Kontaxis and A. Bax, Protein structure determination using molecular fragment replacement and NMR dipolar couplings, *J. Am. Chem. Soc.*, 2000, **122**, 2142–2143.
72. Y. Shen, *et al.*, Consistent blind protein structure generation from NMR chemical shift data, *Proc. Natl. Acad. Sci. U. S. A.*, 2008, **105**, 4685–4690.
73. S. Raman, *et al.*, NMR Structure Determination for Larger Proteins Using Backbone-Only Data, *Science*, 2010, **327**, 1014–1018.
74. F. Delaglio, G. Kontaxis and A. Bax, Protein structure determination using molecular fragment replacement and NMR dipolar couplings, *J. Am. Chem. Soc.*, 2000, **122**, 2142–2143.
75. S. Raman, *et al.*, NMR structure determination for larger proteins using backbone-only data, *Science*, 2010, **327**, 1014–1018.
76. Y. Shen, *et al.*, Consistent blind protein structure generation from NMR chemical shift data, *Proc. Natl. Acad. Sci. U. S. A.*, 2008, **105**, 4685–4690.

77. M. J. Berardi, W. M. Shih, S. C. Harrison and J. J. Chou, Mitochondrial uncoupling protein 2 structure determined by NMR molecular fragment searching, *Nature*, 2011, **476**, 109–113.
78. S. Krauss, C. Y. Zhang and B. B. Lowell, The mitochondrial uncoupling-protein homologues, *Nat. Rev. Mol. Cell Biol.*, 2005, **6**, 248–261.
79. M. Jaburek, *et al.*, Transport function and regulation of mitochondrial uncoupling proteins 2 and 3, *J. Biol. Chem.*, 1999, **274**, 26003–26007.
80. S. Bruschweiler, Q. Yang, C. Run and J. J. Chou, Substrate-modulated ADP/ATP-transporter dynamics revealed by NMR relaxation dispersion, *Nat. Struct. Mol. Biol.*, 2015, **22**, 636–641.
81. Z. Cao and J. U. Bowie, Shifting hydrogen bonds may produce flexible transmembrane helices, *Proc. Natl. Acad. Sci. U. S. A.*, 2012, **109**, 8121–8126.
82. A. Saupe, Recent Results in the Field of Liquid Crystals, *Angew. Chem., Int. Ed. Engl.*, 1968, **7**, 97–112.
83. R. M. Pielak, J. R. Schnell and J. J. Chou, Mechanism of drug inhibition and drug resistance of influenza A M2 channel, *Proc. Natl. Acad. Sci. U. S. A.*, 2009, **106**, 7379–7384.
84. J. L. Lorieau, Partial alignment, residual dipolar couplings and molecular symmetry in solution NMR, *J. Biomol. NMR*, 2019, **73**, 477–491.
85. M. E. Call, *et al.*, The structure of the zetazeta transmembrane dimer reveals features essential for its assembly with the T cell receptor, *Cell*, 2006, **127**, 355–368.
86. J. Jumper, *et al.*, Highly accurate protein structure prediction with AlphaFold, *Nature*, 2021, **596**, 583–589.
87. M. Zweckstetter, NMR hawk-eyed view of AlphaFold2 structures, *Protein Sci.*, 2021, **30**, 2333–2337.